Structural Characterization of a High Affinity Mononuclear Site in the Copper(II)-α-Synuclein Complex

Marco Bortolus,[†] Marco Bisaglia,[‡] Alfonso Zoleo,[†] Maria Fittipaldi,[§]
Maurizio Benfatto,[||] Luigi Bubacco,*[,‡] and Anna Lisa Maniero*[,†]

*Dipartimento di Scienze Chimiche, Università di Padova, via Marzolo, 1, 35131 Padova, Italy,
Dipartimento di Biologia, Università di Padova, via Ugo Bassi 58B, 35121 Padova, Italy,
Laboratorio di Magnetismo Molecolare, Dipartimento di Chimica, Università di Firenze,
Via della Lastruccia 3, 50019 Sesto Fiorentino (FI), Italy, and Laboratori Nazionali di Frascati
dell'INFN, Via Enrico Fermi 40, 00044 Frascati (Roma), Italy*

Received April 20, 2010; E-mail: luigi.bubacco@unipd.it; annalisa.maniero@unipd.it

Abstract: Human α-Synuclein (aS), a 140 amino acid protein, is the main constituent of Lewy bodies, the cytoplasmatic deposits found in the brains of Parkinson's disease patients, where it is present in an aggregated, fibrillar form. Recent studies have shown that aS is a metal binding protein. Moreover, heavy metal ions, in particular divalent copper, accelerate the aggregation process of the protein. In this work, we investigated the high affinity binding mode of truncated aS (1−99) (aS99) with Cu(II), in a stoichiometric ratio, to elucidate the residues involved in the binding site and the role of copper ions in the protein oligomerization. We used Electron Paramagnetic Resonance spectroscopy on the Cu(II)-aS99 complex at pH 6.5, performing both multifrequency continuous wave experiments and pulsed experiments at X-band. The comparison of 9.5 and 95 GHz data showed that at this pH only one binding mode is present. To identify the nature of the ligands, we performed Electron Spin Echo Envelope Modulation, Hyperfine Sublevel Correlation Spectroscopy, and pulsed Davies Electron−Nuclear Double Resonance (Davies-ENDOR) experiments. We determined that the EPR parameters are typical of a type-II copper complex, in a slightly distorted square planar geometry. Combining the results from the different pulsed techniques, we obtained that the equatorial coordination is {N_{Im}, N^-, H_2O, O}, where N_{im} is the imino nitrogen of His50, N^- a deprotonated amido backbone nitrogen that we attribute to His50, H_2O an exchangeable water molecule, and O an unidentified oxygen ligand. Moreover, we propose that the free amino terminus (Met1) participates in the complex as an axial ligand. The MXAN analysis of the XAS k-edge absorption data allowed us to independently validate the structural features proposed on the basis of the magnetic parameters of the Cu(II)-aS99 complex and then to further refine the quality of the proposed structural model.

Introduction

Parkinson disease (PD) is the second most common neurodegenerative disorder in humans and is characterized by the progressive loss of dopaminergic neurons in the *substantia nigra pars compacta* with a consequent decrease of dopamine in its striatal projections.[1] The pathological hallmark of PD is the presence of cytoplasmatic inclusions, protein aggregates named Lewy bodies, in which several molecules have been identified.[2] The most abundant are ubiquitin and fibrillar α-synuclein (aS).[3] Although the role of protein aggregates in causing the disease is still unclear, it remains a central point in the debate on neurodegeneration.[4] A general agreement exists on the fact that

misfolded forms of aS, although not necessarily the insoluble aggregates themselves, are correlated to the pathogenesis. The potential role of different molecular cofactors on the aggregation process has been investigated by post-mortem analyses of brain tissues from patients with PD. The involvement of heavy metal ions in PD was suggested on the basis of the considerable increase in total iron, zinc, and aluminum content observed in the Parkinsonian *substantia nigra* when compared to control tissues.[5,6] Moreover, elevated concentrations of copper were reported in the cerebrospinal fluid of patients with PD,[7] and chronic exposure to copper, iron, lead, and manganese was linked to PD also on the basis of epidemiologic analysis.[8] In vitro experiments confirmed that metal ions can directly increase

[†] Dipartimento di Scienze Chimiche, Università di Padova.
[‡] Dipartimento di Biologia, Università di Padova.
[§] Laboratorio di Magnetismo Molecolare, Dipartimento di Chimica, Università di Firenze.
[||] Laboratori Nazionali di Frascati dell'INFN.
(1) Dauer, W.; Przedborski, S. *Neuron* 2003, *39*, 889–909.
(2) Shults, C. W. *Proc. Natl. Acad. Sci. U.S.A.* 2006, *103*, 1661–1668.
(3) Spillantini, M. G.; Schmidt, M. L.; Lee, V. M.; Trojanowski, J. Q.; Jakes, R.; Goedert, M. *Nature* 1997, *388*, 839–840.
(4) Ross, C. A.; Poirier, M. A. *Nat. Rev. Mol. Cell. Biol.* 2005, *6*, 891–898.

(5) Dexter, D. T.; Wells, F. R.; Lees, A. J.; Agid, F.; Agid, Y.; Jenner, P.; Marsden, C. D. *J. Neurochem.* 1989, *52*, 1830–1836.
(6) Riederer, P.; Sofic, E.; Rausch, W. D.; Schmidt, B.; Reynolds, G. P.; Jellinger, K.; Youdim, M. B. *J. Neurochem.* 1989, *52*, 515–520.
(7) Pall, H. S.; Williams, A. C.; Blake, D. R.; Lunec, J.; Gutteridge, J. M.; Hall, M.; Taylor, A. *Lancet* 1987, *2*, 238–241.
(8) Gorell, J. M.; Johnson, C. C.; Rybicki, B. A.; Peterson, E. L.; Kortsha, G. X.; Brown, G. G.; Richardson, R. J. *Neurology* 1997, *48*, 650–658.

the rate of aS fibril formation.[9,10] A correlation was found between the ability to accelerate fibril formation and the induction of a conformational change: the correlation has been ascribed either to the effective neutralization of the columbic repulsion,[9] or to the stabilization of soluble, partially folded oligomers.[10] The ability of polyvalent metal ions to coordinate proteins in a bridged fashion was proposed as a plausible explanation of the observed oligomer stabilization.[10]

Copper is the most effective ion in promoting aS oligomerization,[9] and, unique among metal ions, its effects are observed at concentration values close to those expected within cells.[11] It is not surprising that the interaction between aS and Cu(II) has been investigated in great depth. Results obtained in time by different investigators were often in contrast with each other. Early data indicated the presence of a large number of independent local copper binding sites in the aS sequence, mainly located in the C-terminal region, with $K_d \approx 60 \ \mu M$.[9] It is now established that most of the previously described binding sites involve nonspecific electrostatic interactions ($K_d \approx 500 \ \mu M$) with charged amino acid side chains in the acidic C-terminal portion of aS.[12,13] A first isothermal titration calorimetry analysis revealed the presence of two high affinity binding sites characterized by dissociation constants for the wild-type protein of 1.7 and 13 μM.[14] More recently, an ICT study by another group provided evidence of the presence of a single copper binding site with a lower dissociation constant ($K_d \approx 42 \ nM$ at pH 7.2 and $K_d \approx 21 \ nM$ at pH 7.4).[15] Using a combination of low- and high-resolution spectroscopic techniques, Rasia and colleagues identified and characterized two distinct tight Cu(II)-binding motifs in aS with dissociation constants in the 0.1 to 50 μM range.[12] The high-affinity copper-binding site was suggested to be located in the N-terminus of the protein, with amino acids 3−9 and 49−52 showing the most prominent effect. The second, lower affinity binding motif was confirmed to be located at the C-terminus in the 110−140 region. In contrast with this report, another work, based on NMR experiments, indicated the presence of two binding sites involving independently the N-terminus of the protein or the histidine residue present in the protein sequence, His50.[13] This latter proposal was supported by another study based on tryptophan fluorescence on four aS mutants containing single tryptophan substitution (F4W, Y39W, F94W, and Y125W) and on the double mutant F4W/H50S.[16] Moreover, studies carried on short aS fragments indicated that the N-terminal region of the protein retains the ability to bind copper also in the absence of His50.[17,18] Nevertheless, potentiometric and spectroscopic studies on modified aS fragments (M^{29}-D^{30}-56) suggested the presence of two dominant binding modes, one containing the

histidine residue.[19] Two independent noninteracting copper binding sites were again reported in a spectroscopic characterization of the Cu(II)-aS complexes.[20] Using a mass spectrometry based approach, the investigators proposed a direct role of Met1 as the anchoring residue for Cu(II) in the high affinity binding site. The second lower-affinity binding motif for Cu(II) ($K_d \approx 50 \ \mu M$) was suggested to be centered around His50.[20] Similar results were obtained in a recent work, based on an EPR analysis carried out on the full length protein and on its H50N mutant.[21] In the presence of a stoichiometric amount of Cu(II), at pH 7.4, a comparable proportion of two distinct binding modes, both typical of type II Cu(II) centers with N and O ligands, was revealed in wild-type aS. This proportion of the two species, based on simulations and deconvolutions of CW EPR spectra, implies a similar Cu(II) affinity for the two sites, and is not in agreement with the difference in the values of the binding constants discussed above.[14]

In the present work, we investigate by advanced EPR techniques and X-ray absorption spectroscopy (XAS) the binding of Cu(II) to the aS99 deletion mutant. Pulsed EPR techniques were used in order to obtain a detailed description of the ligands and the surrounding atoms. The XANES data were analyzed using a recent method, called MXAN, that allows a quantitative structural determination around the absorbing site.[22] Furthermore, CW EPR spectra were obtained to investigate whether the aS99(H50Q) mutant retains the ability to bind Cu(II), also under our experimental conditions.

Our results show the presence of a single Cu(II)-aS99 complex, involving His50 and the N-terminal region of the protein at pH 6.5 and may also shed some light on the mechanism of aS aggregation induced by Cu(II). Copper does not seem to coordinate different aS molecules in a bridged fashion to promote aggregation as previously proposed.[10]

Materials and Methods

Protein Expression and Purification. The aS99 deletion mutant was produced as previously described.[23,24] Briefly, human aS99 cDNA was subcloned into the *Nco*I and *Xho*I restriction sites of the pET28a plasmid (Novagen). Overexpression of the protein was achieved in *E. coli* BL21(DE3) strain, by growing cells in 1 L of LB medium at 37 °C to an OD_{600} of 0.8 followed by induction with 0.3 mM isopropyl β-thiogalactopyranoside for 4 h. After boiling the cell homogenate for 15 min, solid ammonium sulfate was added to the soluble fraction, containing aS99, and the fraction precipitating between 35% and 55% saturation was collected. The pellet was then resuspended, dialyzed, loaded into a 6 mL Resource S column (Amersham Biosciences) and eluted with a NaCl gradient. Finally, the protein was dialyzed against water, lyophilized and stored at −20 °C.

(9) Paik, S. R.; Shin, H. J.; Lee, J. H.; Chang, C. S.; Kim, J. *Biochem. J.* **1999**, *340* (Pt 3), 821–828.

(10) Uversky, V. N.; Li, J.; Fink, A. L. *J. Biol. Chem.* **2001**, *276*, 44284–44296.

(11) Brown, D. R.; Qin, K.; Herms, J. W.; Madlung, A.; Manson, J.; Strome, R.; Fraser, P. E.; Kruck, T.; von Bohlen, A.; Schulz-Schaeffer, W.; Giese, A.; Westaway, D.; Kretzschmar, H. *Nature* **1997**, *390*, 684–687.

(12) Rasia, R. M.; Bertoncini, C. W.; Marsh, D.; Hoyer, W.; Cherny, D.; Zweckstetter, M.; Griesinger, C.; Jovin, T. M.; Fernandez, C. O. *Proc. Natl. Acad. Sci. U.S.A.* **2005**, *102*, 4294–4299.

(13) Sung, Y. H.; Rospigliosi, C.; Eliezer, D. *Biochim. Biophys. Acta* **2006**, *1764*, 5–12.

(14) Bharathi; Rao, K. S. *Biochem. Biophys. Res. Commun.* **2007**, *359*, 115–120.

(15) Hong, L.; Simon, J. D. *J. Phys. Chem. B* **2009**, *113*, 9551–9561.

(16) Lee, J. C.; Gray, H. B.; Winkler, J. R. *J. Am. Chem. Soc.* **2008**, *130*, 6898–6899.

(17) Kowalik-Jankowska, T.; Rajewska, A.; Wisniewska, K.; Grzonka, Z.; Jezierska, J. *J. Inorg. Biochem.* **2005**, *99*, 2282–2291.

(18) Jackson, M. S.; Lee, J. C. *Inorg. Chem.* **2009**, *48*, 9303–9307.

(19) Kowalik-Jankowska, T.; Rajewska, A.; Jankowska, E.; Grzonka, Z. *Dalton Trans.* **2006**, *42*, 5068–5076.

(20) Binolfi, A.; Lamberto, G. R.; Duran, R.; Quintanar, L.; Bertoncini, C. W.; Souza, J. M.; Cervenansky, C.; Zweckstetter, M.; Griesinger, C.; Fernandez, C. O. *J. Am. Chem. Soc.* **2008**, *130*, 11801–11812.

(21) Drew, S. C.; Leong, S. L.; Pham, C. L.; Tew, D. J.; Masters, C. L.; Miles, L. A.; Cappai, R.; Barnham, K. J. *J. Am. Chem. Soc.* **2008**, *130*, 7766–7773.

(22) Della Longa, S.; Arcovito, A.; Girasole, M.; Hazemann, J. L.; Benfatto, M. *Phys. Rev. Lett.* **2001**, *87*, 155501−1155501−4.

(23) Bisaglia, M.; Tessari, I.; Pinato, L.; Bellanda, M.; Giraudo, S.; Fasano, M.; Bergantino, E.; Bubacco, L.; Mammi, S. *Biochemistry* **2005**, *44*, 329–339.

(24) Tessari, I.; Bisaglia, M.; Valle, F.; Samorì, B.; Bergantino, E.; Mammi, S.; Bubacco, L. *J. Biol. Chem.* **2008**, *283*, 16808–16817.

The aS99(H50Q) mutant cDNA was generated by site-directed mutagenesis (QuikChange-Stratagene) using the pET28-aS99 vector as template and the following oligonucleotides for the PCR amplification step:

5′-GAGTGGTGCAAGGTGTGGCAAC-3′

5′-GTTGCCACACCTTGCACCACTC-3′

DNA sequencing was achieved to verify the presence of the mutation. Then, aS99(H50Q) protein was produced following the same protocol used for the wild-type protein. To confirm the identity of the protein, a mass spectrometry measurement was carried out on the protein after the last purification step.

EPR Sample Preparation. Two samples with 0.9:1 Cu(II):aS99 ratio were prepared, one in buffered solution and one in D_2O buffered solution. The copper-containing buffer (pH 6.5) was prepared starting from H_2O or D_2O: the composition was 20 mM 2-(*N*-morpholino)ethanesulfonic (MES), 100 mM NaCl, and 0.45 mM $CuCl_2$. Samples were prepared adding the respective buffer to a weighted aliquot of the lyophilized protein up to a final concentration of 0.5 mM for X-band experiments, and 1 mM for W-band experiments (copper concentrations has been adjusted accordingly).

CW-EPR Experiments. Continuous Wave (CW-) EPR spectra at X-band were recorded using a Bruker ER200D spectrometer equipped with a standard rectangular cavity (ER 4102ST). Experiments were carried out at 110 K using a Bruker VT5113 temperature controller. The W-band CW-EPR spectra were recorded using a Bruker E600 spectrometer equipped with the standard TeraFlex probehead with a TE_{011} cavity. Experiments were carried out at 40 and 60 K, using a Oxford ITC4 temperature controller. Microwave power was accurately selected to avoid signal saturation. CW-EPR spectra have been simulated using the Easyspin program,[25] considering the natural abundance of the two copper isotopes. A quantitation of the copper was made by comparing the value of the double integral of the spectra of both aS99 and aS99(H50Q) copper complexes to that of a standard solution ($CuCl_2$ 0.45 mM, Imidazole 5 mM, MES 20 mM, pH 6.5). The results confirmed that the great majority of the copper in the samples (>90%) partakes of the Cu(II)-aS complex.

Pulsed EPR Experiments. Pulsed EPR experiments were carried out using an X-band ELEXSYS Pulsed EPR Bruker E580D spectrometer, equipped with a dielectric resonator for two-, three-pulse ESEEM (2P-, 3P ESEEM), and HYSCORE experiments, and with an ENDOR dielectric resonator and an ENI A300RF power amplifier for Davies ENDOR experiments. Pulsed experiments were performed at 5 K using an Oxford CF935 liquid helium flow cryostat and an Oxford ITC4 temperature controller. The ESEEM and ENDOR spectra were simulated with a home written suite of programs based on the density matrix formalism of Mims[26] and taking into account an angle selection averaging scheme.[27] The HYSCORE spectrum was simulated using the Saffron routine of the Easyspin program.[25]

2P ESEEM. The 2P ESEEM pulse sequence was $\pi/2-\tau-\pi-\tau$-Echo,[28] with π pulse of 32 ns. The initial delay time τ between the first two pulses was chosen as 200 ns and incremented in steps of 8 ns. A total of 512 points were recorded. The proper phase cycle was applied in order to eliminate contributions from spurious echoes and unwanted artifacts. 2P ESEEM experiments were performed on H_2O and D_2O samples to evidence the contributions arising for exchangeable deuterons coupled to the metal center.[29] The time traces obtained for the two samples were normalized for signal intensity and the envelope of the D_2O sample was divided by the envelope of the H_2O sample.

3P ESEEM. The 3P ESEEM sequence $\pi/2-\tau-\pi/2-T-\pi/2-\tau$-Echo was used.[28] The delay time τ between the first two pulses was chosen as 136 ns, and the time T was varied in steps of 16 ns, starting from 80 ns. A total of 512 points were recorded. Experiments with a τ value of 200 ns were also performed and are reported in the Supporting Information. The proper phase cycle was applied in order to eliminate contributions from spurious echoes and unwanted artifacts. The time traces of the 3P ESEEM experiments were baseline corrected with an exponential decay, time reconstructed, apodized with a Hamming window function, and zero filled to enhance resolution; the resulting time traces were Fourier-transformed and the real part of the FT was taken to produce ESEEM spectra in the frequency domain.

Pulsed ENDOR. The ENDOR experiments were performed using the DAVIES sequence,[28] π-T-$\pi/2-\tau-\pi-\tau$-Echo, with a RF π pulse applied during the delay T. Two different pulse lengths were chosen to detect both ^1H and ^{14}N (160−80−160 ns) or to selectively detect ^{14}N signals (40−20−40 ns).[30] The RF pulse was 12 μs long for both experiments.

HYSCORE. HYSCORE spectra were recorded using the sequence $\pi/2-\tau-\pi/2-t_1- \pi-t_2- \pi/2-\tau-$Echo, where the echo is measured as a function of t_1 and t_2.[28] The duration of the $\pi/2$ and π pulses was 16 and 32 ns, respectively. The time τ between first and second pulse was 200 ns, the time increment in t_1 and t_2 was 16 ns, and 64 × 64 points were collected. The HYSCORE time traces were baseline corrected with a third-order polynomial, then apodized with a Hamming window function, and zero filled to enhance resolution; the resulting time traces were 2D Fourier-transformed and the absolute value of the FT was taken to produce the frequency HYSCORE spectrum.

XANES. The XANES (X-ray Absorption Near Edge Structure) measurements were performed at the ESRF synchrotron facility, at the GILDA beamline. The Cu K-edge XANES signals were collected in fluorescence mode by a seven-element CANBERRA Ge detector. A Si (311) crystal was used as a monochromator. The energy range was from 8700 to 9700 eV, the calibration of energy was performed by means of a copper foil reference. Only the XANES part of the spectra, i.e., from 8900 to 9200 eV, was analyzed to have the best energy to noise ratio and strongest sensitivity to the three-dimensional structure around the absorber. Here the energy resolution was 0.3 eV, with a counting time of 6 s/point. Samples are in the same chemical conditions of those used for the magnetic resonance experiments previously described.

The XANES data analysis has been performed by using the MXAN method[22] capable to fit the energy region from the edge up to 200 eV above threshold in terms of selected structural parameters. The main novelty of this approach lies in the fact that the total photon absorption cross section is calculated exactly without any series expansion. In this way, all of the multiple scattering contributions are properly taken into account and the absorption coefficient is directly given as a function of the energy, allowing an immediate fit of the experimental data. The effectiveness of this approach has been already tested successfully both in a number of test cases[31] and in the definition of unknown structures[32] (and references therein). The MXAN method performs the minimization of the residual function R_{sq} defined as follows:

(25) Stoll, S.; Schweiger, A. *J. Magn. Reson.* **2006**, *178*, 42−55.
(26) Mims, W. B. *Phys. Rev. B* **1972**, *5*, 2409−2419.
(27) (a) Hurst, G. C.; Henderson, T. A.; Kreilick, R. W. *J. Am. Chem. Soc.* **1985**, *107*, 7294−7299. (b) Henderson, T. A.; Hurst, G. C.; Kreilick, R. W. *J. Am. Chem. Soc.* **1985**, *107*, 7299−7303.
(28) Schweiger, A.; Jeschke, G. *Principles of Pulse Electron Paramagnetic Resonance*; Oxford University Press: New York, 2001.
(29) Dikanov, S. A.; Tsvetkov, Y. D. *Electron Spin Echo Envelope Modulation (ESEEM) spectroscopy*; CRC Press:Boca Raton, FL, 1992.
(30) Thomann, H.; Bernardo, M. *Methods Enzymol.* **1993**, *227*, 118−161.
(31) Hayakawa, K.; Hatada, K.; D'Angelo, P.; Della Longa, S.; Natoli, C. R.; Benfatto, M. *J. Am. Chem. Soc.* **2004**, *126*, 15618−15623.
(32) Bubacco, L.; Spinazze, R.; Della Longa, S.; Benfatto, M. *Arch. Biochem. Biophys.* **2007**, *465*, 320−327.

$$R_{sq} = \sum_{i=1}^{m} \frac{[(y_i^{th} - y_i^{exp})\varepsilon_i^{-1}]^2}{m}$$

where m represent the number of experimental data, y_i^{th} and y_i^{exp} are the theoretically computed and experimental measured values of the absorption coefficient, respectively. ε_i represent our estimate of the experimental error, considered constant in the fitting procedure. In our case, it was considered equal to 1% of the experimental edge jump. Details of the MXAN procedure are described elsewhere.[22]

The cluster of atoms used in the fitting procedure includes atoms up to 7.0 Å from the absorber and the muffin-tin radii are chosen according to the Norman criterion with an overlapping optimized during the fit procedure. The number of atoms of the cluster has been chosen on a convergence criterion since larger clusters do not add any further feature to the simulated spectra.

Results

CW-EPR. CW-EPR spectra were measured at X and W band, to evidence the possible presence of more than one single mode of Cu(II)-aS99 binding. Figure 1 shows the CW X band (left) and W band (right) EPR spectra of the sample in frozen aqueous buffer solution, along with simulations. Line broadening from g strain[33] is evident in the W band spectrum particularly in the $g_{||}$ region, preventing the resolution of the Cu(II) hyperfine parallel components, while the X band line width is mainly determined by unresolved superhyperfine couplings of ligand and surrounding nuclei. The spectra obtained at both frequencies were satisfactorily simulated considering a single set of magnetic parameters, an indication that only one Cu(II)-aS99 complex is present. The following values for the g and copper hyperfine tensors have been used in the simulations: $g_{xx} = 2.048$, $g_{yy} = 2.053$, $g_{zz} = 2.229$ and $A_{xx} = A_{yy} = 32$ MHz, $A_{zz} = 540$ MHz (the hyperfine values are reported for the ^{63}Cu isotope).

The high frequency spectrum could be simulated only allowing a moderate deviation of the g tensor from axial symmetry and using different line widths for the three g tensor components. The g tensor values indicate a Cu(II) ground state largely $3d_{x^2-y^2}$, with some admixture of $3d_{z^2}$, which causes the slight deviation of g from axial symmetry. According to the established Blumberg-Peisach correlations,[34] the g_{zz} and A_{zz} values fall in the range expected for a 2N2O or 3N1O copper coordination in the equatorial plane. If we consider the ground state to be essentially $3d_{x^2-y^2}$, then the g and copper hyperfine tensors can be used to estimate the unpaired electron population in the copper orbital.[35,36] We obtained the value of 0.76, within the range of 0.7−0.8 estimated for tetra-coordinated Cu(II) complexes with mixed nitrogen and oxygen ligands.[37] Additionally, we prepared the H50Q mutant of aS99, and obtained the CW-EPR spectrum of the Cu(II)-aS99(H50Q) complex. The spectrum and the magnetic parameters obtained from the simulation are reported in the Supporting Information, SI.

3P ESEEM. Three pulse ESEEM spectra, along with simulations, are shown in Figure 2: they were obtained at 5 K at field positions A, B, and C indicated by arrows in Figure 1. The spectra show peaks in the 0−5 MHz range, characteristic for a
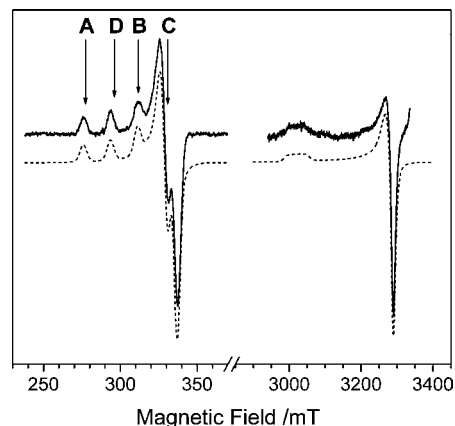

Figure 1. CW-EPR spectra of Cu(II):aS99 0.9:1 molar ratio in MES buffer at pH = 6.5 (continuous line), with their simulations (dashed line). The X-band spectrum (left) was obtained with the following parameters: $T = 110$ K, microwave frequency 9.4563 GHz, microwave power 20 mW, modulation amplitude 0.5 mT. The W-band spectrum (right) was obtained with the following parameters: $T = 60$ K, microwave frequency 94.2 GHz, microwave power 16 μW, modulation amplitude 0.5 mT. The letters show the resonance positions where the ESEEM (A, B, C, see Figure 2) or Davies ENDOR (C, D, see Figures 3 and S1 of the Supporting Information) experiments have been performed.
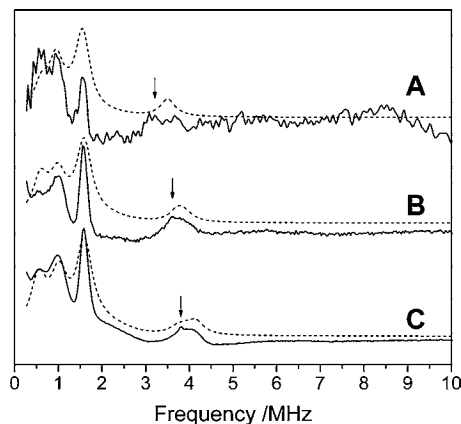

Figure 2. Real-part FT of the 3P ESEEM traces of Cu(II):aS99 0.9:1. $T = 5$ K, delay time $\tau = 136$ ns. The three experiments (continuous line) were performed at the three different field positions (A, B, C) shown in Figure 1. The parameters obtained from the simulations (dashed lines) are reported in Table 1. The arrows indicate the position of the free Larmor frequency of the ^{23}Na ($\nu = 3.944$ MHz at 3.5 mT) originating from the buffer.

^{14}N with predominantly isotropic hyperfine coupling close to the cancellation conditions.[29] The narrow low frequency lines correspond to nearly pure ^{14}N quadrupolar transitions occurring in one electron spin manifold, while the broad feature at ∼4.00 MHz, which moves with the magnetic field setting, arises from the $\Delta m_I = \pm 2$ transition taking place within the other electron spin manifold. No additional signals (combination bands) are seen in the range 2−4 MHz, suggesting that only a single weakly coupled nitrogen is observed.[38] The simulations shown in Figure 2 were obtained assuming the ^{14}N hyperfine tensor as axial: the fitting parameters are collected in Table 1.

The ^{14}N hyperfine and quadrupolar tensor values in Table 1 are comparable with those found for the remote nitrogen of histidine ligands in type 1 and type 2 Cu(II) proteins or Cu(II)

(33) Cannistraro, S. *J. Phys.* **1990**, *51*, 131–139.
(34) Peisach, J.; Blumberg, W. E. *Arch. Biochem. Biophys.* **1974**, *165*, 691–708.
(35) Fujimoto, M.; Janecka, J. *J. Chem. Phys.* **1971**, *55*, 1152–1157.
(36) (a) Maki, A. H.; McGarvey, B. R. *J. Chem. Phys.* **1958**, *29*, 31–34. (b) Maki, A. H.; McGarvey, B. R. *J. Chem. Phys.* **1958**, *29*, 35–38.
(37) Getz, D.; Silver, B. L. *J. Chem. Phys.* **1974**, *61*, 630–638.

(38) McCracken, J.; Pember, S.; Benkovic, S. J.; Villafranca, J. J.; Miller, R. J.; Peisach, J. *J. Am. Chem. Soc.* **1988**, *110*, 1069–1074.
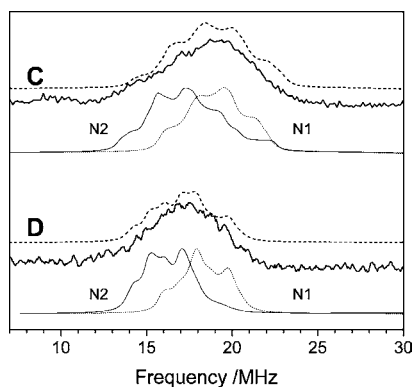
Figure 3. ^{14}N Davies ENDOR of Cu(II)-aS99 in H_2O at 5 K, RF pulse 12 μs; microwave π pulse 40 ns. The experiments were performed at the field positions C (top), and D (bottom) of the EPR spectrum of Figure 1. Experimental spectra (continuous line), are shown below the simulations (dashed line); these have been obtained as 1:1 sum of the individual nitrogen simulations shown in thin lines (left, N2, right, N1, see text).

Table 1. Hyperfine and Quadrupolar Parameters of the Remote Histidine ^{14}N Nucleus Obtained from the Simulation of the 3P-ESEEM Spectra (see Figure 2)^a

	A_{iso} (MHz)	$|T_\perp|$ (MHz)	θ^b	$|e^2qQ/h|$ (MHz)	η	β^b
N_{his}	1.57 ± 0.02	0.15 ± 0.02	$80° \pm 10°$	1.65 ± 0.02	0.7 ± 0.02	$40° \pm 10°$

^{a} Hyperfine tensor principal values: $A_{iso}-T_\perp|$, $A_{iso}-|T_\perp|$, and $A_{iso}+2|T_\perp|$, where A_{iso} and $T_\perp = -1/2\ T_{||}$, are the isotropic and the perpendicular dipolar components. The quadrupolar tensor components are $Q_{xx} = -e^2qQ(1-\eta)/4h$, $Q_{yy} = -e^2qQ(1+\eta)/4h$, $Q_{zz} = 2e^2qQ/4h$, expressed in terms of the quadrupolar coupling constant e^2qQ/h and of the asymmetry parameter η. ^{b} The two sets of Euler angles relating the hyperfine and quadrupolar tensor frames to the g tensor frame are not fully specified, as the ESEEM spectra are sensitive only to θ and β angles,[51] that define the orientations of the maximum hyperfine ($A_{iso}+2|T_\perp|$) and quadrupolar (Q_{zz}) components with respect to the g_{zz} direction.

imidazole and Cu(II) histidine model systems,[39−50] thus identifying His50 as the Cu(II) ligand responsible for the signals in the ESEEM spectra. It has been found that the quadrupolar parameters of the imidazole remote nitrogen in Cu(II) complexes

(39) Bolm, C.; Martin, M.; Gescheidt, M.; Palivan, C.; Neshchadin, D.; Bertagnolli, H.; Feth, M.; Schweiger, A.; Mitrikas, G.; Harmer, J. *J. Am. Chem. Soc.* **2003**, *125*, 6222–6227.
(40) Bubacco, L.; van Gastel, M.; Groenen, E. J. J.; Vijgenboom, E.; Canters, G. W. *J. Biol. Chem.* **2003**, *278*, 7381–7389.
(41) Colaneri, M. J.; Peisach, J. Cap.15 In *Biomedical EPR—Part A: Free Radicals, Metals, Medicine, and Physiology*; Eaton, S. S., Eaton, G. R., Berliner, L. J. Eds.; Kluwer/Plenum: New York, 2005; Vol. 23, pp 229−282.
(42) Elliott, S. J.; Randall, D. W.; Britt, R. S.; Chan, S. I. *J. Am. Chem. Soc.* **1998**, *120*, 3247–3248.
(43) Lu, J.; Bender, C. J.; McCracken, J.; Peisach, J.; Severns, J.; McMillin, D. R. *Biochemistry* **1992**, *31*, 6265–6272.
(44) McCracken, J.; Desai, P. R.; Papdopoulos, N. J.; Villfranca, J. J.; Peisach, J. *Biochemistry* **1988**, *27*, 4133–4137.
(45) Coremans, J. W. A.; Poluektov, O. G.; Groenen, E. J. J.; Canters, G. W.; Nar, H.; Messerschmidt, A. *J. Am. Chem. Soc.* **1996**, *118*, 12141–12153.
(46) van Gastel, M.; Coremans, J. W. A.; Jeuken, L. J. C.; Canters, G. W.; Groenen, E. J. J. *J. Phys. Chem. A* **1998**, *102*, 4462–4470.
(47) McCracken, J.; Peisach, J.; Dooley, D. *J. Am. Chem. Soc.* **1987**, *109*, 4064–4072.
(48) Gubriel, R. J.; Peoples, R.; Doan, P. E.; Cline, J. F.; McCracken, J.; Peisach, J.; Hoffman, B. M.; Valentine, J. S. *Inorg. Chem.* **1993**, *32*, 1813–1819.
(49) van Dam, P. J.; Reijerse, E. J.; van der Meer, M. J.; Guajardo, R.; Mascharak, P. K.; de Boer, E. J. *Appl. Magn. Reson.* **1996**, *10*, 71–86.
(50) Bender, C. J.; Peisach, J. *J. Chem. Soc., Faraday Trans.* **1998**, *94*, 375–386.

are correlated to the hydrogen bonding environment of the nitrogen.[51,52] In this frame, the quadrupolar values determined for the Cu(II)-aS99 complex, in particular the value of $\eta = 0.7$,[53,54] indicate that the remote nitrogen is likely involved in a weak hydrogen bond. Moreover, the principal axes system of the quadrupolar tensor is correlated to the local symmetry, with one axis normal to the imidazole plane and another one in the plane, parallel to the N−H bond.[45,55−57] The axis corresponding to the maximum quadrupolar value was found to be normal to the imidazole plane in many cases.[45,57] A 90° rotation to an in-plane direction was interpreted as an indication of a lower N−H orbital occupancy of the remote nitrogen, which may reflect the presence of a strong hydrogen bonding interaction.[45,53,55,56] As the quadrupolar parameters of the remote histidine nitrogen in Cu(II)-aS99 suggest the presence of a weak hydrogen bond, we conclude that the direction corresponding to the maximum quadrupolar coupling (Q_{zz}) could be normal to the imidazole plane. The angle of $40° \pm 10°$ between the g_{zz} direction (perpendicular to the coordination plane) and the Q_{zz} direction, obtained from the simulations of the ESEEM spectra, suggests a tilt of the imidazole ring with respect to the copper ligand plane.

^{14}N **Pulsed ENDOR.** Pulsed ENDOR experiments were performed with different pulse lengths to resolve signals deriving from weak and strong hyperfine interactions. The spectra recorded with short pulse lengths (40/20/40 ns) at positions C and D of the EPR spectrum (see Figure 1) are shown in Figure 3. They are typical for strongly coupled ^{14}N nuclei directly bound to Cu(II).[58−60] Using short microwave pulses, the ENDOR signals of weak interactions, mainly deriving from the ligand or environment protons, are suppressed and the signals corresponding to stronger interactions are enhanced.[30,61] The ENDOR signals in Figure 3 should derive from the Cu(II) interaction with at least two directly coordinated ^{14}N nuclei, as inferred from the g and copper hyperfine values using the Blumberg−Peisach diagrams.[34] The signals of Figure 3 are rather featureless, a characteristic often found in similar cases,[58−60] and encompass a narrow range of about 11 and 9 MHz, for the $g_\perp$ and $g_{||}$ positions, respectively. However, they show a significant dependence on the magnetic field setting, with the spectrum recorded at the $g_\perp$ position extending to higher frequencies with respect to the spectrum recorded at the $g_{||}$ position. All of these findings indicate that the two (or three) ^{14}N have similar and relatively anisotropic hyperfine tensors, with the axes corresponding to the maximum hyperfine coupling lying in the coordination plane. This latter evidence is consistent with the interaction of copper with equatorial ^{14}N nuclei, for

(51) Jiang, F.; Karlin, K. D.; Peisach, J. *Inorg. Chem.* **1993**, *32*, 2576–2582.
(52) Jiang, F.; McCracken, J.; Peisach, J. *J. Am. Chem. Soc.* **1990**, *112*, 9035–9044.
(53) Colaneri, M. J.; Vitali, J.; Peisach, J. *Biochemistry* **2000**, *39*, 584–591.
(54) Jiang, F.; Peisach, J.; Ming, L. L.; Que, L.; Chen, V. J. *Biochemistry* **1991**, *30*, 11437–11445.
(55) Mcdowell, C. A.; Naito, A.; Sastry, D. L.; Cui, Y. U.; Sha, K.; Yu, S. X. *J. Mol. Struct.* **1989**, *195*, 361–381.
(56) Colaneri, M. J.; Peisach, J. *J. Am. Chem. Soc.* **1992**, *114*, 5335–5341.
(57) Ashby, C. I. H.; Cheng, C. P.; Brown, T. I. *J. Am. Chem. Soc.* **1978**, *100*, 6057–6063.
(58) Van Camp, H. L.; Sands, R. H.; Fee, J. A. *J. Chem. Phys.* **1981**, *75*, 2098–2107.
(59) Van Doorslaer, S.; Cereghetti, G. M.; Glockshuber, R.; Schweiger, A. *J. Phys. Chem. B* **2001**, *105*, 1631–1639.
(60) Utschig, L. M.; Astashkin, A. V.; Raitsimring, A. M.; Thurnauer, M. C.; Poluektov, O. G. *J. Phys. Chem. B* **2004**, *108*, 11150–11156.
(61) Gemperle, C.; Schweiger, A. *Chem. Rev.* **1991**, *91*, 1481–1506.

which the largest value of the hyperfine tensor is expected to occur in the direction of the Cu−N vector.

The ENDOR spectra were simulated by assuming the contribution of two ^{14}N nuclei with a 1:1 intensity ratio: both ^{14}N are characterized by an axial dipolar tensor with the principal axis of the maximum coupling in the coordination plane. The strong field dependence of the ENDOR spectra guided the simulation: the spectrum in Figure 3D, as a result of the orientation selection, is lacking the contribution of the perpendicular component of the ^{14}N hyperfine tensors; the comparison between the spectra in Figure 3, parts C and D, allowed a first estimate of the nitrogen hyperfine values that were later refined in the final simulations. As the experimental spectra are poorly resolved, we assumed for the two ^{14}N nuclei identical quadrupolar parameters, chosen within the range of the literature data (reported in the SI), regarding the directly coordinated ^{14}N of histidine and other types of ^{14}N nuclei that could serve as copper ligands. The ENDOR simulations, shown in Figure 3 are obtained with the following parameters: for N1 (A_{iso} 37.6 MHz, $|T_\perp|$ 2.1 MHz), for N2 (A_{iso} 34.0 MHz, $|T_\perp|$ 3.0 MHz) and for both nitrogens $|e^2qQ/h|$ = 2.0 MHz and η = 0.5.

As starting hypothesis, the assignment of the N1, N2 nitrogens to the histidine and to an amino or amido group was made by evaluating the p/s ratio of the bonding orbitals of the two nitrogens (see the SI for the expressions).[60] For an amino nitrogen, a p/s ratio higher than that of an amido or imidazole nitrogen is expected, since the bonding orbitals are mainly sp^3 for amino and sp^2 for amido and imidazole nitrogens.[62,63] Indeed, it was reported that amino nitrogens coordinated to Cu(II) have a p/s ratio around 5.0.[35,55,64,65] We estimated a p/s ratio of ∼1.6 for N1 and ∼1.8 for N2; these values are very far from the expected value for an amino group as Cu(II) ligand. Furthermore, the hyperfine coupling constants of amino nitrogens are, in general, smaller than those determined for N1 and N2, due to the higher p character of the bonding orbital of a pyramidal nitrogen.[55,62−68] The two nitrogens more likely correspond to the coordinated nitrogen of His50 and to a deprotonated amido nitrogen of the backbone. In order to assign N1 or N2 to the directly coordinated nitrogen of His50, the ratio of the ^{14}N hyperfine coupling constants between the directly coordinated and remote nitrogens were determined. From the literature, the value of this ratio in several Cu-His complexes ranges form 20 to 22.[55,56,58,69,70] For the N1 and N2 nitrogens of Cu-aS99 the value is about 24.0 and 21.6, respectively, suggesting that N2 is more likely to correspond to the directly coordinated nitrogen of His50 and N1 to an amido nitrogen of the backbone.

The hyperfine values obtained from the simulation of our poorly resolved ENDOR spectra allowed only an educated guess
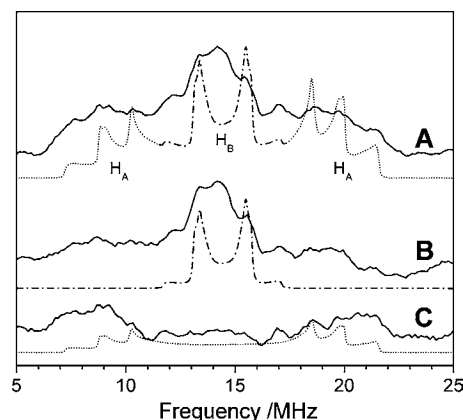

Figure 4. (A) Davies ENDOR profile of Cu(II)-aS99 exchangeable protons, and its simulation, sum of the traces for protons H$_A$ (dotted line, wings, B) and protons H$_B$ (dash-dot line, center, C), see text. The experimental spectrum in (A) is the sum of the individual traces shown in (B) and (C) with continuous lines. In (B) the difference, H$_2$O minus D$_2$O, of the ENDOR selective spectra with π = 160 ns. In (C) the difference, H$_2$O minus D$_2$O, of the ENDOR selective spectra with π = 40 ns. The ENDOR experiments were performed at 5 K, at the observer position C (see Figure 1).

on the nature of the ligands, however they led to a good starting structure for the fitting of the XAS data (see below).

^{1}H Pulsed ENDOR. ENDOR spectra with pulse lengths 160−80−160 ns were recorded at position C ($g_\perp$) of the EPR spectrum in samples prepared in H$_2$O and D$_2$O buffers, to identify the signals from exchangeable protons. We specifically searched for evidence of water molecules binding to Cu(II). The ENDOR spectra in H$_2$O and D$_2$O buffers are shown in the SI (Figure S3A of the SI). The difference (H$_2$O minus D$_2$O), which contains only signals from exchangeable protons, is reported in Figure 4B: it is dominated by the strong peaks of weakly coupled protons with hyperfine couplings in the range 0−5 MHz, but the presence of less intense features, extending on a broad frequency range, are indicative of protons with much larger hyperfine couplings. As the use of short microwave pulses results in the suppression of very small hyperfine couplings, ENDOR spectra with pulse length 40−20−40 ns were recorded for the H$_2$O and D$_2$O samples (see Figure S3B of the SI), in order to highlight, in their difference spectrum, the signals from the exchangeable protons with relatively large hyperfine couplings. The difference spectrum, reported in Figure 4C, shows a pair of broad features, centered around the proton Larmor frequency (ν_P = 14.4 MHz), corresponding to hyperfine couplings in the range 8−14 MHz. These couplings are in the expected range for the interaction of Cu(II) with the protons of equatorially bound water molecules.[71−73] We simulated the ENDOR pattern by assuming a proton hyperfine tensor with rhombic symmetry, to reproduce the broad ENDOR pattern: the principal axis corresponding to the largest hyperfine value was taken along the Cu−H direction, considering a H$_2$O molecule with the oxygen atom in the equatorial plane. The dotted line in Figure 4C shows the ENDOR simulation obtained with the following values for the isotropic coupling and the dipolar coupling tensor of the proton(s) (in the following

(62) Iwaizumi, M.; Kudo, T.; Kita, S. *Inorg. Chem.* **1986**, *25*, 1546–1550.
(63) Scholl, H. J.; Huettermann, J. *J. Phys. Chem.* **1992**, *96*, 9684–9691.
(64) McDowell, C. A.; Naito, A. *J. Magn. Reson.* **1981**, *45*, 205–222.
(65) McDowell, C. A.; Naito, A.; Sastry, D. L.; Cui, Y.; Sha, K. *J. Phys. Chem.* **1990**, *94*, 8113–8118.
(66) Fujimoto, M.; McDowell, C. A.; Takui, T. *J. Chem. Phys.* **1979**, *70*, 3694–3701.
(67) Calvo, R.; Oseroff, S. B.; Abache, H. C. *J. Chem. Phys.* **1980**, *72*, 760–767.
(68) Wartewig, S.; Bottcher, P.; Windsch, W. *Chem. Phys.* **1981**, *58*, 211–225.
(69) Van Camp, H. L.; Sands, R. H.; Fee, J. A. *Biochim. Biophys. Acta, Protein Struct. Mol. Enzymol.* **1982**, *704*, 75–89.
(70) Coremans, J. W. A.; Poluektov, O. G.; Groenen, E. J. J.; Canters, G. W.; Nar, H.; Messerschmidt, A. *J. Am. Chem. Soc.* **1997**, *119*, 4726–4731.

(71) Huffman, D. L.; Huyett, J.; Outten, F. W.; Doan, P. E.; Finney, L. A.; Hoffman, B. M.; O'Halloran, T. V. *Biochemistry* **2002**, *41*, 10046–10055.
(72) Fann, Y. C.; Ahmed, I.; Blackburn, N. J.; Boswell, J. S.; Verkhovskaya, M. L.; Hoffman, B. M.; Wikstrom, M. *Biochemistry* **1995**, *34*, 10245–10255.
(73) Atherton, N. M.; Horsewill, A. *J. Mol. Phys.* **1979**, *37*, 1349–1361.

indicated as H_A): $A_{iso} = \mp 1.7$ MHz, $(T_{aa}, T_{bb}, T_{cc}) = \pm (16.1, 9.5, 6.6)$ MHz; based on the quality of the simulations we estimate a mean error of ± 0.15 MHz for the tensor components.

The hyperfine tensor values of proton(s) H_A are larger than those obtained for the protons of water molecules equatorially bound to Cu(II) in the $Cu(II)(H_2O)_6$ complex in crystals of a Tutton salt, whose magnetic parameters are usually taken as reference for water molecules coordinated to Cu(II).[73] Nevertheless, the isotropic and anisotropic couplings of protons H(a) can be explained if a slightly higher spin density is delocalized on the equatorial water molecule in the Cu(II)-aS99 complex with respect to the $Cu(II)(H_2O)_6$ reference system (see SI for details).

In addition to the signals of protons H_A, the difference spectrum in Figure 4B clearly show two pairs of features separated by about 5.5 and 2.2 MHz, respectively, whose line shapes are indicative of a nearly axial proton interaction. The dash-dot line in Figure 4B shows the simulation of this pattern, obtained with the following parameters (in the following this proton(s) will be indicated as H_B): $A_{iso} = 0.2$ MHz, $(T_{aa}, T_{bb}, T_{cc}) = (-2.3, -2.9, +5.2)$ MHz; based on the quality of the simulations we estimate a mean error of ± 0.05 MHz for the tensor components. The axis corresponding to the largest dipolar value was taken as perpendicular to the coordination plane, and a copper-proton distance of ~ 0.29 nm is obtained from the value $T_{cc} = 5.2$ MHz, by using the point dipole approximation. A possible attribution of these proton signals will be presented in the discussion. The total simulation, comprising protons H_A and H_B, has been superimposed to the spectrum obtained by adding traces 4B and 4C.

In order to have independent assessment of the parameters identified for the proton tensors from the ENDOR spectra, 2P ESEEM and HYSCORE experiments were performed at the $g_\perp$ position of the EPR spectrum.

2P ESEEM Experiments. Two-pulse ESEEM spectra were acquired on the H_2O and D_2O samples and the ESEEM trace collected for the D_2O sample was divided by the ESEEM trace of the H_2O sample, recorded under identical conditions. This ratio cancels out all of the modulations but those from exchangeable protons,[74] and it provides a method to monitor water molecules coordinated to metal ions, even in the presence of considerable ESEEM signals from weakly coupled nitrogens.[29] Figure 5A reports the pattern resulting from the D_2O/H_2O ratio: it shows intense modulations at the frequency of about 2.2 MHz (modulation period ~ 450 ns), the Larmor frequency of deuterium (for a magnetic field value of 3380 G), and at the sum combination frequency of about 4.4 MHz. Figure 5B shows the simulation of the ESEEM ratio, obtained by using the hyperfine tensor derived from the ENDOR spectra, and attributed to protons of a water molecule bound to copper in equatorial position (protons H_A). Trace C is a simulation obtained by including both the proton hyperfine tensors H_A and H_B obtained from ENDOR. The proton hyperfine values were properly scaled for deuterium, the deuterium quadrupolar parameters were chosen as $e^2qQ = 0.22$ MHz and $\eta = 0.10$, and hyperfine and quadrupolar tensors were taken as coaxial.[75] The simulations in Figure 5B/C reproduce well the experimental pattern, giving support to the hyperfine tensors H_A and H_B obtained from ENDOR.

¹H HYSCORE. HYSCORE experiments were performed at $g_\perp$ position of the EPR spectrum (position C in Figure 1) for
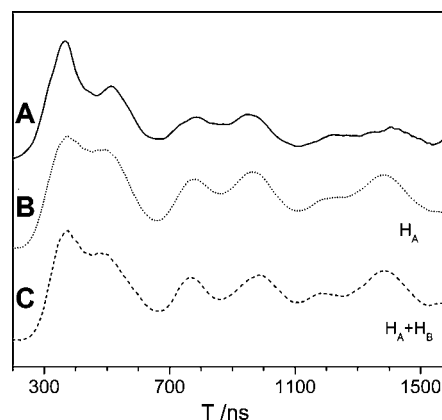

Figure 5. (A) Ratio between the 2P ESEEM traces of the samples in D_2O and H_2O taken at 5 K, ($\pi = 32$ ns). (B) simulation obtained with proton tensor H_A (dashed line); (C) simulation obtained by including both proton tensor H_A and proton tensor H_B (dotted line). The experiments were performed at observer position C (see Figure 1).
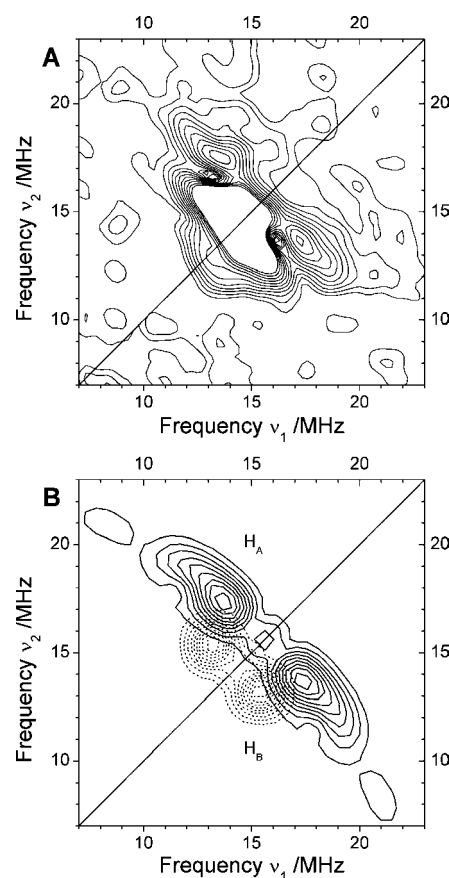

Figure 6. (A) Proton region of the HYSCORE spectrum and (B) the simulation obtained with the proton tensor H_A (continuous lines) and proton tensor H_B (dashed lines). The experiment was performed at observer position C (see Figure 1).

the Cu-aS99 sample in aqueous buffer. The proton region of the HYSCORE spectrum is reported in Figure 6A: it shows two well-defined ridges shifted from the antidiagonal at ν_P, indicating protons with a relevant dipolar hyperfine coupling.[28,76,77] For an axial hyperfine tensor, the $T_\perp$ dipolar value can be estimated

(74) Mims, W. B.; Davis, J. L.; Peisach, J. *Bioph. J.* **1984**, *45*, 755–766.
(75) Hegg, E. L.; Whiting, A. K.; Saari, R. E.; McCracken, J.; Hausinger, R. P.; Que, L., Jr. *Biochemistry* **1999**, *38*, 16714–16726.
(76) Poeppl, A.; Kevan, L. *J. Phys. Chem.* **1996**, *100*, 3387–3394.
(77) van Gastel, M.; Bubacco, L.; Groenen, E.; Vijgenboom, E.; Canters, G. W. *FEBS Lett.* **2000**, *474*, 228–232.
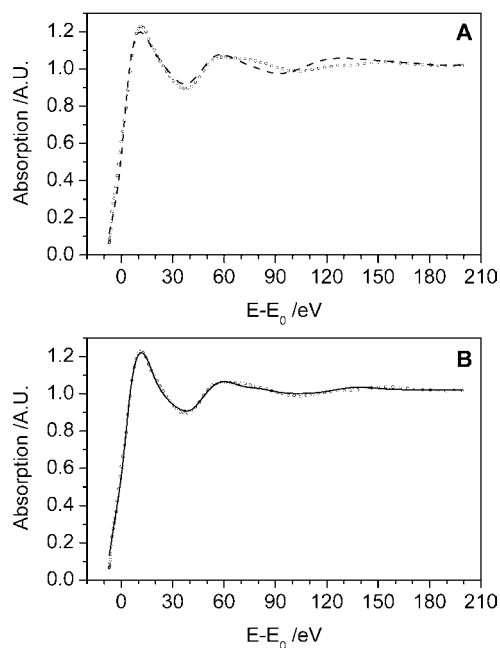
Figure 7. Cu K-edge XANES data of the of Cu(II)-aS99 complex (hollow dots). (A) The dashed line shows the simulation generated with the parameters of the starting structure (Figure S3 of the SI). (B) The continuous line shows the MXAN simulation leading to the optimized structure (Figure 8). All parameters for the simulations are reported in Table 2. The energy is scaled relative to the edge energy, $E_0 = 8985$ eV.

from the maximum vertical shift of the ridge pattern: from spectrum of Figure 6A we obtained $T_\perp \approx 8$ MHz, in accord with the dipolar tensor of protons H_A. A further verification of the ENDOR data was obtained by the HYSCORE simulations performed with the hyperfine tensors H_A and H_B: the calculated spectra, reported in Figure 6B, as solid contour plot lines for H_A and dashed contour plot lines for H_B, are in very good agreement with the experimental profiles.

XAS. As it will be described in the discussion, the interpretation of the data obtained from the EPR experiments presented above provides the rationale to design a structural model of the Cu(II)-aS99 complex, that was then used as starting structure in the fitting procedure of the XAS data. The type of information used in the generation of such model is more related to the type of ligand and strength of the metal ligand interaction rather than to the coordination geometry that is actually the information that is expected from the MXAN analysis. The coordination geometries and the bond lengths used for the proposed starting model refer to published structural properties of Cu(II) complexes with paramagnetic interaction comparable to those observed for Cu(II)-aS99. The starting model is reported in Figure S4 of the SI: two oxygen and two nitrogen atoms define the equatorial plane, while a third nitrogen defines the z-axis of the cluster (see Discussion). The atom labeled W_{exc} of the figure represents the oxygen of the water molecule.

The comparison between the experimental XANES data and the theoretical calculation obtained by using the structural model derived from the EPR experiments is presented in Figure 7A. Points represent the experimental data and the energy is reported in relative scale with $E_0 = 8985$ eV. Although the presence of several discrepancies, the agreement between theory and experiment can be considered remarkable for a starting structure calculation, indicating the reliability of the structural model coming from the magnetic resonance experiments. To arrive at the best fit parameters the choice was made to move the first

neighbors ligands changing the bond lengths (Cu–N/O distances) and their relative angles with the z-axis that was kept fixed during the optimization procedure. During the movement of the copper ligand atoms, the other atoms that compose the ligand molecules were considered as a rigid body. The comparison between the experimental data and the theoretical calculation at the best fit condition is reported in Figure 7B. The agreement between the two curves is now quite good in the whole energy range as corroborated by a marked decrease of the error function R_{sq} from 5.31 to 1.29. The structural results are summarized in Table 2 and the final model is depicted in the Figure 8. Bond lengths in Table 2 are reported with the statistical errors as evaluated by MXAN by the MINUIT subroutine of the MINUIT package.

In the Supporting Information, we present an additional fitting obtained considering the structure proposed in the literature for the Cu(II)-aS complex that involves the His50 ring and the N-terminal region of the protein in the equatorial plane ("Mode 2" in ref 21). The R_{sq} of this structure, after the optimization of the bond lengths, was significantly worse ($R_{sq} = 2.44$) than the value obtained for the model we propose and shown in Figure 8.

To pinpoint the contribution of the axial ligand in the fitting procedure, starting from the best-fit parameters used to generate the fitting curve reported in Figure 7B, the R_{sq} value was calculated as a function of the Cu–N distance of the axial ligand: the results of this procedure are reported in Figure 9. A broad minimum is observed for a range of distances from 0.20 to 0.22 nm, but more importantly the quality of the fit is decreasing sharply at increasing distance values, suggesting that the presence of the axial ligand is germane to the quality of the fit.

Discussion

The unique specificity of Cu(II) binding to aS, when compared with all other transition metal ions, triggered several studies aimed to unravel its binding mode.[78] A large number of independent nonspecific copper binding sites, located in the C-terminal region, have been described and these could represent a potential interfering factor in the structural characterization of the aS complex. To circumvent this problem, this work was focused on the 1–99 deletion mutant of aS.

The descriptions of the copper-specific binding site(s) that emerged in the literature were often contradictory. An high-affinity copper-binding site was first suggested to be located in the N-terminus of the protein involving His50, at pH 6.5.[12] After this work, many studies pointed to the central role played by the free N-terminus as the anchoring group in the coordination of the Cu(II) ion.[13,16–20] Another investigation, based mainly on the interpretation of the CW EPR spectra of Cu(II)-aS and Cu(II)-aS(H50N), described two distinct binding modes with similar Cu(II) affinity at pH 7.4, both located in the N-terminal region.[21] "Mode 1" was assigned to a {NH_2, N^-, β-COOH, H_2O} binding mode, involving coordination of the N-terminal amine of Met1 and the deprotonated backbone amide and carboxylate side chain of Asp2. Although the ligands that define the first coordination sphere for "Mode 2" remained unresolved, a 2N2O or 3N1O coordination was suggested. However, the participation of His50 to the coordination "Mode 2" was confirmed in a pulsed EPR experiment.[21] In this frame, it is

(78) Bisaglia, M.; Tessari, I.; Mammi, S.; Bubacco, L. *NeuroMol. Med.* **2009**, *11*, 239–251.

Table 2. Copper-Ligand Distances (nm) for the First Coordination Shell for the Starting Structure and the Best-Fit Distances Obtained from the MXAN Simulation of the K-Edge Absorption Data (Figure 7)

structure	R_{sq}	Cu—N (Met1)	Cu—N2 (His50)	Cu—N1 (His50)	Cu—O	Cu—W$_{exc}$
starting	5.31	0.220	0.210	0.202	0.202	0.201
optimized	1.29	0.220 ± 0.007	0.196 ± 0.046	0.192 ± 0.007	0.219 ± 0.061	0.193 ± 0.008

important to mention that, just below a stoichiometric Cu(II): aS99 ratio at pH 6.5, none of our data suggest the presence of more than one type of Cu(II)-aS99 complex. In fact, multiple band CW-EPR spectra were simulated using the same set of magnetic parameters, and, as will be discussed later, also the fitting of the XAS data was performed using one single binding mode. Our results are in agreement with those reported in ref 12 where, at pH 6.5, a dominant species was found. We deem that the value of pH plays a prominent role in shaping the binding site; indeed strong pH dependence was previously found: the CW-EPR spectra of Cu(II)-aS greatly change going from pH 7.4 to 5.0.[21]

The results from the pulsed EPR experiments converge to a structural model in which a single binding mode exists with a 2N2O equatorial coordination as shown in Figure 8. The two nitrogen ligands are the δ imino nitrogen from His50 and a backbone α amido nitrogen that we propose to derive from His50, whereas the two oxygen ligands are a water molecule and, possibly, a carbonyl group. Here we suggest that the
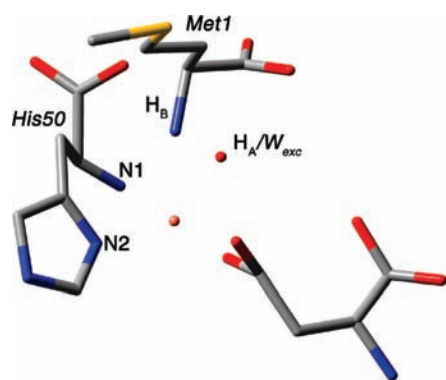
Figure 8. The proposed Cu(II) coordination site in aS. The atoms have been labeled according to the names used in Table 2: N1 and N2 are the nitrogen atoms of the His50 residue, H$_A$/W$_{exc}$ are the protons of the equatorially coordinated water molecule, H$_B$ are the protons bound to the nitrogen atom of Met1 axially coordinated to copper.
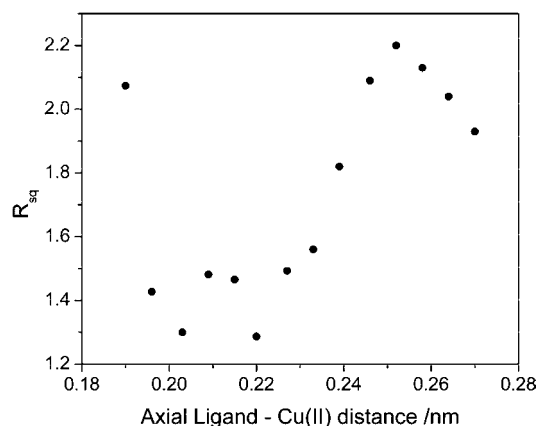
Figure 9. Dependence of the quality of the simulation of the K-edge spectra on the axial ligand distance from the Cu(II) metal center. All atoms of the axial ligand were moved as a single rigid body while all other parameters were maintained constant to the values presented in Table 2.

N-terminal amine group of Met1 also partakes in the same binding site of His50 as an axial ligand to Cu(II). The ESEEM experiments clearly identify His50 as one of the ligand in which the coordinated nitrogen is likely to be the δ imino nitrogen of the same residue (N2 in Figure 8), as suggested also by the analysis of the ENDOR data. The assignment of the second coordinated nitrogen (N1 in Figure 8) is based mostly on the ENDOR spectra analysis that suggests a backbone amide. For a peptide in solution, the ionization of amido hydrogens normally occurs between pH 13 and 15, but the process is significantly enhanced in the presence of Cu(II) when the imidazole ring of the histidine residue is available to act as an anchor for the metal ion. As an example, in the presence of stoichiometric concentration of Cu(II), the peptide AcGlyGlyHis shows a pK_{a1} of 6.5, and the peptide AcGlyGly HisGly a pK_{a1} of 6.0.[79] Then, in neutral or slightly acidic solutions, using histidine as an anchor, Cu(II) is able of deprotonating neighboring backbone amido nitrogens in peptides and in unstructured regions of proteins.[80] The preferred coordination is to the N terminal amido nitrogen of the histidine residue, which results in the formation of the stable six membered chelate ring with the histidine N^δ and the backbone N^α of the histidine.[79,81] Coordination of the amido nitrogen to the C terminus of the histidine produces a less stable seven atoms ring. However, an example of this less favored C-terminal coordination is provided by the octarepeat region of the prion protein (PHGGGWGQ).[82–84] It should be mentioned that the proline preceding the histidine residue serves as a break point, directing the observed C-terminal amide coordination.[85] In the same protein in the nonoctarepeat binding site at His96, lacking the proline residue (GGGTHNQ), Cu(II) coordinates with the preferred mode to backbone amides on the N terminal side of His96.[86,87]

On the basis of the previous considerations, we propose the backbone amido nitrogen of His50 as the amido nitrogen

(79) Sundberg, R. S.; Martin, R. B. *Chem. Rev.* **1974**, *74*, 471–517.
(80) Sigel, H.; Martin, R. B. *Chem. Rev.* **1982**, *82*, 385–426.
(81) Kroneck, P. M. H.; Vortisch, V.; Hemmerich, P. *Eur. J. Biochem.* **1980**, *109*, 603–612.
(82) Aronoff-Spencer, E.; Burns, C. S.; Avdievich, N. I.; Gerfen, G. J.; Peisach, J.; Antholine, W. E.; Ball, H. L.; Cohen, F. E.; Prusiner, S. B.; Millhauser, G. L. *Biochemistry* **2000**, *39*, 13760–13771.
(83) Chattopadhyay, M.; Walter, E. D.; Newell, D. J.; Jackson, P. J.; Aronoff-Spencer, E.; Peisach, J.; Gerfen, G. J.; Bennett, B.; Antholine, W. E.; Millhauser, G. L. *J. Am. Chem. Soc.* **2005**, *127*, 12647–12656.
(84) Burns, C. S.; Aronoff-Spencer, E.; Dunham, C. M.; Lario, P.; Avdievich, N. I.; Antholine, W. E.; Olmstead, M. M.; Vrielink, A.; Gerfen, G. J.; Peisach, J.; Scott, W. G.; Millhauser, G. L. *Biochemistry* **2002**, *41*, 3991–4001.
(85) Garnett, A. P.; Viles, J. H. *J. Biol. Chem.* **2003**, *278*, 6795–6802.
(86) Burns, C. S.; Aronoff-Spencer, E.; Legname, G.; Prusiner, S. B.; Antholine, W. E.; Gerfen, G. J.; Peisach, J.; Millhauser, G. L. *Biochemistry* **2003**, *42*, 6794–6803.
(87) Gralka, E.; Valensin, D.; Porciatti, E.; Gajda, C.; Gaggelli, E.; Valensin, G.; Kamysz, W.; Nadolny, R.; Guerrini, R.; Bacco, D.; Remelli, M.; Kozlowski, H. *Dalton Trans.* **2008**, *5207*, 5219.
(88) Cornelius, J. B.; McCracken, J.; Clarkson, R. B.; Belford, R. L.; Peisach, J. *J. Phys. Chem.* **1990**, *94*, 6977–6982.
(89) Binolfi, A.; Rasia, R. M.; Bertoncini, C. W.; Ceolin, M.; Zweckstetter, M.; Griesinger, C.; Jovin, T. M.; Fernandez, C. O. *J. Am. Chem. Soc.* **2006**, *128*, 9893–9901.
(90) Sandal, M.; Valle, F.; Tessari, I.; Mammi, S.; Bergantino, E.; Musiani, F.; Brucale, M.; Bubacco, L.; Samorì, B. *PLoS Biol.* **2008**, *6*, e6.

identified as a copper ligand from the ENDOR spectra of aS99. The presence of a single six atoms ring is also supported by the XAS analysis that is particularly sensitive to the nuclei in close proximity of the scattering center.[22] Indeed we considered a second model which was suggested for the Cu(II)-aS complex at pH 7.4,[21] where two chelating rings are present, and this model produced a worse fitting of the XAS data (see the SI).

NMR data of spin relaxation induced by the paramagnetic Cu(II), showed that the regions of aS mainly affected by Cu(II) binding are around His50. Accordingly, the ESEEM and ENDOR results presented here indicate copper binding to the nitrogen of His50 and to its backbone amido nitrogen. However, the N terminus (residues 3−9) is also reported as a region affected by copper binding. As the broadening effect of a type II Cu(II) site on the NMR resonances reaches ∼1.1 nm from the Cu(II) location,[12] the NMR relaxation data do not allow one to distinguish between an axial or equatorial coordination. The previous NMR observations can be reconciled to the data presented in this study if the amino terminal group is assumed to act as axial ligand of copper. An axially bound nitrogen interacts with Cu(II) more weakly than equatorial ligands, then, in principle, it could be seen in ESEEM spectra. However, its ESEEM modulation is expected to be very shallow and not likely observable, especially in the presence of the strong contribution from the remote nitrogen of an equatorially bound histidine, with interaction close to the cancellation regime, as in our case.[54,71,88] Moreover, in the proton ENDOR spectra we have detected proton(s) (H_B in Figure 8) characterized by an hyperfine interaction that is mainly dipolar and has an axial symmetry, with the main axis nearly perpendicular to the coordination plane of the complex. The amine protons of a NH_2 group axially coordinated to copper should give rise to such a hyperfine interaction, and the copper-proton distance of ∼0.29 nm, inferred from the proton(s) H_B dipolar interaction, provides a copper−nitrogen distance of ∼0.24 nm, in good agreement with the XAS data for the axial ligand reporting as upper end of the best fitting copper−nitrogen distances ∼0.22 nm.

The two oxygen ligands in the Cu(II)-aS99 complex are not directly detectable. However, strong evidence is provided both by ENDOR and HYSCORE for the presence of a bound equatorial water molecule detectable for its protons (H_A in Figure 8). The presence of this solvent molecule, likely to be exchangeable, bound to an equatorial position poses an interesting question on a potential catalytic activity of copper when bound to aS.

The ensemble of magnetic resonance experiments converged to a structural model that allows defining the chemical nature of the copper ligands and the strength of their interactions, but lacks a direct evaluation of both bond lengths and precise coordination geometry. The MXAN analysis of the XAS data allowed, first, to independently validate the structural features proposed on the basis of the magnetic properties of the Cu(II)-aS99 complex and then to further refine the quality of the proposed structural model. A relevant point refers to the contribution of the axial ligand in the fitting procedure; as mentioned in the result section, starting from the best-fit parameters used to generate the fitting curve reported in Figure 7B, the R_{sq} value was calculated as a function of the Cu−N distance of the axial ligand. The presence of a minimum that encompasses a range of distances going from 0.20 to 0.22 nm

does not allow to independently asses the exact position of the axial ligand but strongly supports its presence and its assignment (see Figure 9).

A number of studies appeared where copper binding was retained upon mutation of His50, suggesting that Met1 is the main anchoring residue for copper binding.[13,18,21] To verify whether or not copper binding is maintained at pH 6.5 in the absence of His50, we prepared the H50Q mutant of aS99. The CW-EPR spectrum of the Cu(II)-aS99(H50Q) complex is significantly different from that of the Cu(II)-aS99 complex (see the SI). The quantitation of copper in the EPR spectrum shows that aS99(H50Q) binds copper quantitatively at this pH. From the simulation of the CW-EPR spectrum, we found that again only a single species is present, but the magnetic properties of the complex indicated that the binding mode changes relative to aS99. The g and copper hyperfine tensors are very similar to those previously described for the H50A mutant at pH 7.4.[21]

One last consideration relates to the mechanisms by which the interactions between α-synuclein and Cu(II) promote the aggregation events that are still not understood. Experimental evidence indicated that Cu(II) promotes the nucleation, but not the growth phase, suggesting that the Cu(II)-bound form of α-synuclein is more prone to nucleate than the uncomplexed protein.[12] Furthermore, 70% to 90% of the Cu(II) used in the aggregation assay was incorporated into the α-synuclein aggregates.[89] The presence of Cu(II) in the fibrils indicates that the protein aggregates in its copper-bound form. At least in the time frame analyzed in this work, the Cu(II) does not act as aggregating factor by recruiting His residues from different aS molecules since multiple histidine coordination was not observed. Instead, the copper binding to the high-affinity site of α-synuclein might be a critical step in the aggregation process inducing a local order in the protein structure, an hypothesis that has been proposed in the literature for the Cu(II)-aS interaction on the basis of single molecule AFM experiments.[90] This process, in vivo, might start a cascade of structural alterations that generate a pool of α-synuclein molecules more prone to aggregate.

Supporting Information Available: CW-EPR spectra of the Cu(II)-aS99(H50Q) complex, all 3P-ESEEM spectra, discussion of literature data on quadrupolar parameters, expression for the p/s ratios, all DAVIES ENDOR spectra, starting and alternative models for the MXAN fitting, and dissociation constants for the Cu(II)-aS99 and Cu(II)-aS99(H50Q) complexes. This material is available free of charge via the Internet at http://pubs.acs.org.

JA103338N